

# PURDUE OPTICAL GROUND STATION SENSOR TASKING OPTIMIZATION AND MULTI-TARGET TRACKING WITH A MULTI-LAYER PHD FILTER

Abdulrahman Abdrabou, Juan Gutierrez, and Carolin Frueh

Purdue University, School of Aeronautics and Astronautics, 701 W. Stadium Avenue, West Lafayette, IN 47906, USA  
Email: {saleh3, gutier23, cfrueh}@purdue.edu

## ABSTRACT

In recent years, a combination of technology maturation and space accessibility has resulted in an increase in the number of launches, which continues to exacerbate the problem of maintaining and increasing Space Situational Awareness (SSA) for safe space operation. A critical objective of SSA activities is the generation and maintenance of a space object catalog. An observation strategy and the characterization of tracklets from the collection of images are among a set of initial key elements that contribute to the continued accuracy of a catalog. In this paper, a follow-up sensor tasking optimization algorithm is used to determine observation schedules that maximize object coverage for tracking objects in the Geosynchronous (GEO) orbital region. To generate observation schedules, the sensor tasking algorithm considers several visibility conditions and prioritizes unobserved objects to obtain the optimal viewing directions. The algorithm utilizes prior knowledge of cataloged objects to initialize viewing directions. A set of observation schedules is generated for the Purdue Optical Ground Station (POGS) and executed for two nights. Detections are obtained using two different image processing techniques, conservative and non-conservative. Detection association is performed to evaluate the sensor tasking with a prior object using the Mahalanobis Distance Association (MDA) process and Multi-Layer PHD filter composed of two steps. The first step forms tracklets from a collection of image sets with a Gaussian mixture PHD (GM-PHD) filter in the orthogonal image plane. The second step of the Multi-Layer PHD filter utilizes a labeled classical approach for the full orbital GM-PHD filter to determine the number of observed objects.

Keywords: Multi-Target Tracking, FISST, Probability Hypothesis Density Filter, Sensor Tasking, GEO Catalog, Optical Observations.

## 1. INTRODUCTION

The exponential growth of the total number of space objects in the near-Earth region poses significant chal-

lenges to space operations and safety [5, 14]. These objects include active and operational satellites, as well as space debris. Accurate detection, tracking, identification, and characterization of these objects are crucial for maintaining comprehensive Space Situational Awareness. According to the latest European Space Agency (ESA) space environment report, there are currently more than 36,000 objects cataloged and tracked [14]. About 9,100 of these objects are active payloads, and the remaining are pieces of debris larger than 10 centimeters in size. There are currently almost 1 million non-cataloged objects that are between 1 and 10 centimeters in size. It is also estimated using ESA's space debris environment model, MASTER, that there are 128 million objects between 1 millimeter and 1 centimeter in size [14, 35].

The increase in the population of objects shows the importance and need for regular observations to update available information about their orbits and maintain tracks over time. Optical observations generated by telescopes provide measurements of brightness and directional information in the form of right ascension and declination angles. To generate and maintain a space object catalog, sensor tasking observation strategies are used. The observation strategies can be categorized into two methods, a survey and a follow-up [34, 40, 41]. In the survey observation strategy, parts of the sky are scanned for the detection of new objects, where no prior information is available. Follow-up observations are planned according to the objects for which orbital information is available [28].

The development of sensor tasking algorithms is an integral part of the maintenance of space object catalogs. Earlier studies [4, 40, 41] laid the groundwork by proposing survey strategies to maintain space object catalogs without requiring prior information on object trajectories. The follow-up sensor tasking has also been investigated in [19, 31, 34, 39] to keep track of cataloged objects. The optimization and practical implementation of the sensor tasking are crucial to maximize the use of ground-based telescopes while adhering to real-world observability constraints.

A necessary step in the chain of executing a schedule of observations is the evaluation of the tasked-optimized objects according to a prior catalog. However, objects

are non-resolved in ground-based observations, and there is the occurrence of missed detections, and false detection or clutter. Clutter is a result of the release of photo-electrons from charged particles impinging the detector, among other sources, and does not correspond to the detection of an actual object.

There are several ways of validating the success of sensor tasking. One way is to compare the scheduled with the actual detected objects. In order to facilitate such a comparison, the observations need to be processed and associated, either to each other and/or to the scheduled objects. Two methods of validation are explored, where the first is based on the detections in the single image and can be done with maximum likelihood, Mahalanobis distance association [6, 25, 26]. The second validation method is a more comprehensive approach which can be performed with multi-target tracking (MTT). In MTT, the number of objects or cardinality alongside their states is estimated, solving the data-to-object association problem implicitly or explicitly.

Historically, two main research approaches are used to explore the MTT regime: the track-based approach and the population-based approach. Track-based approaches associate the measurements explicitly with the single targets to form a track. The track of an object is inferred from a sequence of observations collected over time. The individual track of the corresponding object is represented with appropriate probabilistic information [7, 12, 38]. Popular track-based examples are the Multiple Hypothesis Tracking (MHT) [8, 11, 38] and Joint Probability Data Association (JPDA) introduced in [16]. A more holistic probabilistic approach led to the development of multi-target algorithms within a Random Finite Set (RFS) framework, where a random object is described by random size and elements, corresponding to the number of targets and their states, respectively. The entity exists in the absence of measurements and gives a fully probabilistic description of the scene. Mahler [32] uses RFS to formulate the Probability Hypothesis Density (PHD) filter as a solution to the multi-target problem posed in a Bayesian Filtering Framework, which defines the population of targets as a single RFS [32, 33].

A Multi-Layer PHD filter [18] partitions the multi-target problem into two steps. The first step is performed on the orthogonal image plane, where the short series of collected images and the respective detections are utilized to build tracklets. The second step of the problem utilizes the resulting tracklets to perform an update on the prior object catalog.

This paper explores a sensor tasking framework and facilitates validation using two different image processing schemes and two different detection association methods.

## 2. SENSOR TASKING OPTIMIZATION

The sensor tasking algorithm used in this paper and the observation campaign with a real-life telescope is implemented to create optimal observation schedules that include where and when to point a sensor. The sensor tasking algorithm used is based on the follow-up tasking strategy. The algorithm can be used for a single sensor or a multi-sensor framework. The sensor tasking formulation can be expressed as follows [17, 19, 20]:

$$\max(A) = \sum_{g=1}^l \sum_{f=1}^{m_g} \left( \sum_{i=1}^n \mu \cdot P_d \cdot d \right) \quad (1)$$

where  $\mu$  represents the urgency value for each object  $i$ , which allows the algorithm to prioritize unobserved objects.  $P_d$  is the probability of detection of the object  $i$ .  $d$  is the probability that object  $i$  falls within the Field of View (FOV) of sensor  $g$ .  $A$  is the total probable number of objects observed given that the equation contains stochastic variables.  $l$  is the total number of sensors observing in the observation window,  $m_g$  is the total number of observations made by each sensor and  $n$  is the total number of available objects. To implement the sensor tasking algorithm from Equation (1), a greedy optimizer is used to choose the optimal viewing direction. Other optimizers have been explored, but performance to computational runtime of the greedy optimizer has been favored for efficiency, making it applicable to real-time sensor tasking [29, 30].

A commonly used state representation form is the Two-Line Element (TLE) catalog format provided by the USSTRATCOM Space-Track catalog [42] due to its availability. The sensor tasking is performed independently of detection success, and is hence a fixed-schedule open-loop method. Fixed-schedule methods are known to not perform as well as the flexible-schedule feedback methods. However, currently the former are more feasible in most real-world applications.

## 3. OPTICAL VISIBILITY CONDITIONS

Effective object observation requires careful consideration of various environmental and operational factors. To ensure high-quality data collection and optimize sensor performance, a comprehensive set of visibility restrictions was applied to enable a more efficient operational sensor tasking. For instance, sensors typically have a certain minimum elevation, such that any object below that threshold would not be observed.

### 3.1. Moon Separation

Moon glare can degrade image quality and hinder object detection. The angular distance to the center of the Moon

from the observer's perspective,  $\theta_{OOM}$ , can be expressed as:

$$\theta_{OOM} = \arccos(\hat{\rho}_m \cdot \hat{\rho}_O) \quad (2)$$

where  $\hat{\rho}_m$  is the unit vector of the range of the Moon from an observer and  $\hat{\rho}_O$  is the unit vector of the range of the object.

### 3.2. Earth's Shadow

To determine if an object is inside the Earth's shadow, the angular radius of the Earth and Sun from the object is needed. The umbra angle can be expressed as:

$$\theta_{umbra} = \theta_{\oplus-Radius} - \theta_{\odot-Radius} \quad (3)$$

where  $\theta_{\odot-Radius}$  is the angular radius of the Sun from the object and  $\theta_{\oplus-Radius}$  is the angular radius of the Earth from the object. An object is considered in Earth's shadow if the Earth-Object-Sun angle is smaller than or equal to  $\theta_{umbra}$ .

### 3.3. Galactic Plane

To minimize interference from dense star fields, particularly crucial for southern hemisphere sensors, separation from the galactic north and south is desired. This condition can be applied by converting galactic coordinates of the North and South Galactic poles to the J2000 frame.

To convert from Right Ascension (RA) and Declination (DEC) ( $\alpha$  and  $\delta$  respectively), in J2000 to galactic coordinates ( $l, b$ ) or vice versa, the following equations can be used from Binney and Tremaine [10]:

$$\sin(b) = \cos(\delta) \cos(\delta_G) \cos(\alpha - \alpha_G) + \sin(\delta) \sin(\delta_G) \quad (4)$$

$$\sin(l_{NGP} - l) \cos(b) = \cos(\delta) \sin(\alpha - \alpha_G) \quad (5)$$

$$\cos(l_{NGP} - l) \cos(b) = \sin(\delta) \cos(\delta_G) - \cos(\delta) \sin(\delta_G) \cos(\alpha - \alpha_G) \quad (6)$$

where  $\alpha_G$  and  $\delta_G$  are the RA, DEC of the North Galactic Pole (NGP) respectively, and  $l_{NGP}$  is the longitude of the North Celestial Pole (NCP).

$$\alpha_G = 192.85948^\circ \quad (7)$$

$$\delta_G = 27.12825^\circ \quad (8)$$

$$l_{NGP} = 122.93192^\circ \quad (9)$$

### 3.4. Limiting Magnitude

The limiting magnitude of a sensor represents the faintest apparent magnitude of an object that can be detected by it. This threshold is influenced by various factors, such as background noise, atmospheric attenuation, and exposure time. Understanding the limiting magnitude is critical for

evaluating the performance of optical sensors in detecting objects under different observational conditions. An approximation on how to calculate limiting magnitude is as follows [21]:

$$mag_{limit} = mag_{sky} + 5 \cdot \log_{10} \left( \frac{D}{D_{exit}} \right) \quad (10)$$

where  $mag_{sky}$  is the limiting sky magnitude which represents the background brightness,  $D_{exit}$  is the diameter of the exit pupil of the optical sensor, and  $D$  is the diameter of the aperture. It is important that all units used are consistent; typically, millimeters are used.

## 4. DETECTION ASSOCIATION

A reliable method is needed to associate all the object detections made in the images to evaluate the performance and success of the observation schedules generated by the sensor tasking algorithm. Two association methods are implemented in this work, the Mahalanobis Distance Association (MDA) and the Multi-Layer PHD filter, to correlate the detections produced using two image processing techniques.

### 4.1. Two Image Processing Techniques

To obtain detections from the images captured by a sensor, two image processing techniques are used: a conservative and a non-conservative method. In the conservative processing, false positive detections are kept at a minimum, at the cost of false negative detections. The method is based on strict detection thresholding [27]. The non-conservative method favors keeping false negatives to a minimum, at the cost of, at times, a large number of false positive detections. The non-conservative processing is based on convolution methods [27, 28].

### 4.2. Covariance Information

For catalogs that do not provide or have incomplete covariance information, making it difficult to quantify the uncertainty in the propagated position and velocity states, studies have empirically estimated these uncertainties for specific orbital regimes [13]. In particular, previous analyses have characterized the uncertainty of objects in the Space-Track TLE catalog's Geosynchronous Earth Orbit (GEO) population [22].

To account for the absence of second moment information, each propagated TLE object has an assumed  $N(\mu, \Sigma)$ , where  $\mu$  is the mean and  $\Sigma$  is the covariance of the distribution. The largest uncertainty being in the in-track direction [6, 22]. The covariance in the In-Track,

Cross-Track, Out-Of-Plane (ICO) frame can be approximately represented as follows:

$$\Sigma_{ICO} = \begin{bmatrix} \sigma_s^2 & 0 & 0 \\ 0 & \left(\frac{\sigma_s}{\sigma_c}\right)^2 & 0 \\ 0 & 0 & \left(\frac{\sigma_s}{\sigma_o}\right)^2 \end{bmatrix} \quad (11)$$

$$\tilde{\sigma}_c = \frac{\sigma_s}{\sigma_c} \quad (12)$$

$$\tilde{\sigma}_o = \frac{\sigma_s}{\sigma_o} \quad (13)$$

where  $\sigma_s$  represents the standard deviation term in the in-track direction,  $\sigma_c$  is the standard deviation in the cross-track direction, and  $\sigma_o$  is the standard deviation in the out-of-plane direction [6]. The in-track standard deviation is set to  $\sigma_s = 100$  km, based on the assumption that potential measurements will be within 100 km of the TLE object [6]. This choice also mitigates biases introduced by extremely large covariance matrices. The values for the standard deviations in cross-track and out-of-plane are given by  $\tilde{\sigma}_c = 5.608$  and  $\tilde{\sigma}_o = 5.663$ , respectively, derived from Monte Carlo simulations modeling the propagation of the covariance [6].

### 4.3. Mahalanobis Distance Association (MDA)

The Mahalanobis distance is a statistical measure of the distance between a point and a distribution [1]. The Mahalanobis distance,  $d$ , between a point  $y$  and the Gaussian distribution  $N(\mu, \Sigma)$  can be expressed as follows [1]:

$$d^2 = (y - \mu)\Sigma^{-1}(y - \mu)^T \quad (14)$$

The covariance matrix in Equation (11) needs to be rotated to the image plane frame, which is based on RA and DEC. This transformation between frames is performed using Jacobian matrices as a linearization into the observation space of the image plane.

A threshold is applied to identify potential matches from the catalog of objects. Objects with  $d^2$  values below this threshold are considered potential candidates for this observation measurement. This threshold is chosen based on the assumed statistical distribution of the residuals, ensuring that potential candidates fall within a region of high probability density. The threshold is selected heuristically to balance the removal of unlikely candidates while keeping potential matches [6]. A threshold of  $1 \cdot 10^6$  is found to work effectively.

### 4.4. Multi-layer PHD Filter

The Multi-Layer PHD filter is composed of two steps, the first step is the implementation of the image plane PHD. The second step consists of the implementation of a data-driven PHD filter, where the birth is integrated into the measurement update step [23] incorporating classical

orbit determination in contrast to an admissible regions approach. In this paper, the evaluation of the sensor tasking is done only with a prior set of TLE object catalog. Therefore, the full orbital PHD filter in sensor tasking evaluation application does not utilize birth.

The classical PHD filter is a solution to the multi-target problem posed in a Bayesian framework to estimate the cardinality and their states. The PHD filter is a first-order approximation of the full Finite Set Statistics (FISST) proposed by Mahler [32], therefore the leanest version of FISST-based filters.

For the integrated detection and tracking problem in this paper, the RFS of the multi-target state is represented by  $X = \{\mathbf{x}_1, \dots, \mathbf{x}_n\}$ . In the example of a space object,  $\mathbf{x}_i$  can describe the position and velocity states of the target  $i$  for the cardinality of  $|X| = n$  objects, and  $\mathbf{x} \in \mathbb{R}^6$  is the single-target state space. Similar definitions apply to the set-valued measurement  $Z = \{z_1, \dots, z_m\}$  with  $z_i$  as the single-target measurement with  $|Z| = m$  number of measurements or sensor returns and  $z \in \mathbb{Z}$  is the measurement space at a given time  $k + 1$ . For example, for optical the measurement can be described by angles and angle rates  $z \in \mathbb{R}^4$ .

The PHD filter propagates the first-order moment of the multi-target filtering density  $D_{k|k}(\mathbf{x})$ , also known as the intensity function [32], [44]. The prediction step of the classical PHD filter involves the following assumptions: (1) each object is independent and the dynamics can be modeled by Markov transition density  $f_{k+1|k}(\mathbf{x}|\mathbf{x}')$  with prior  $\mathbf{x}'$  and posterior  $\mathbf{x}$ ; (2) the survival process on each object can be modeled by a Bernoulli process with known probability  $p_S$  at each time-step; (3) new objects are born independent of the existing targets, with a known birth process pdf  $b_{k+1|k}(\mathbf{x})$ . Note: spawning is not taken into account in this work. The classical PHD filter prediction for the multi-target probability hypothesis density  $D_{k|k}(\mathbf{x})$  is [32]:

$$D_{k+1|k}(\mathbf{x}) = b_{k+1|k}(\mathbf{x}) + \int p_S(\mathbf{x}')f_{k+1|k}(\mathbf{x}|\mathbf{x}')D_{k|k}(\mathbf{x}')d\mathbf{x}' \quad (15)$$

The assumptions for the measurement update step for the classical PHD filter are: (4) each object produces at most one measurement, where the set of measurements  $Z_{k+1}$  is produced by the union between measurements produced by previous objects and the clutter process  $Z = Z_{\text{object}} \cup Z_{\text{clutter}}$ ; (5) the multi-target prior of the objects is Poisson distributed with variance  $\lambda_{\text{prior}}$ :  $f_{k+1|k}(X|Z) = \exp(-\lambda_{\text{prior}}) \prod_{\mathbf{x} \in X} \lambda_{\text{prior}} \cdot f_{k+1|k}(\mathbf{x}|Z)$ ; (6) there exists a known single target measurement likelihood function  $f_{k+1|k+1}(z|\mathbf{x})$  based on the object state  $\mathbf{x}$  and a single measurement  $z$ , respectively; (7) a probability of detection is known and can be state-dependent, which is modeled as Bernoulli process based on the object state  $p_D(\mathbf{x}) := p_D(\mathbf{x}, \mathbf{x}_{\text{sensor}})$  and the sensor characteristics that include pointing direction and field of view  $\mathbf{x}_{\text{sensor}}$ ; (8) the false alarm clutter rate can be modeled as a Poisson distribution with variance  $\lambda$  and spatial distribution  $c(z) = c(z|\mathbf{x}_{\text{sensor}})$ , which may depend on sensor

characteristics  $\mathbf{x}_{\text{sensor}}$ . The classical PHD filter measurement update is formulated as [32]:

$$D_{k+1|k+1}(\mathbf{x}) = (1 - p_D(\mathbf{x})) \cdot D_{k+1|k}(\mathbf{x}) + p_D(\mathbf{x}) \cdot \sum_{\mathbf{z} \in \mathcal{Z}} \frac{f_{k+1|k+1}(\mathbf{z}|\mathbf{x}) D_{k+1|k}(\mathbf{x})}{\lambda c(\mathbf{z}) + \int p_D(\mathbf{x}) f_{k+1|k}(\mathbf{z}|\mathbf{x}') D_{k+1|k}(\mathbf{x}') d\mathbf{x}'}$$
 (16)

The application of the classical PHD filter for the orthogonal image plane is given in Section 4.4.1. The application of the full orbital PHD filter is described in Section 4.4.2.

#### 4.4.1. Orthogonal Image Plane PHD Filter

The first step in the Multi-Layer process utilizes a short series of images separated by a few seconds, where each  $k$ -th image contains a set of detections  $\tilde{Z}^{(k)} = \{\tilde{z}_1, \dots, \tilde{z}_o\}$  with  $\tilde{z}_i \in \mathbb{R}^2$  and cardinality  $|\tilde{Z}^{(k)}| = o$ . The multi-target state is represented by  $Z = \{z_1, \dots, z_e\}$ , with  $z \in \mathbb{R}^4$  and cardinality  $|Z| = e$ . The state is composed  $z_i = (\alpha, \delta, \dot{\alpha}, \dot{\delta})$ , corresponding to the right ascension, declination, and their respective rates [23].

The orthogonal image plane PHD filter utilizes a Gaussian mixture application with linear dynamics. The Gaussian mixture assumption provides negligible inaccuracies from the use of the Gaussian distribution in spherical coordinates. The linear dynamics assumption is justified for high-altitude orbits where the series of images span a small fraction of the orbit. However, further adaptations can be easily implemented for lower-altitude orbits. The filter does not employ catalog data or any prior information and each short image series is processed independently. The initial Gaussian mixture prepared at the beginning of each image series is produced by uniformly sampling positions on the image plane, while the rates are determined from a pre-analysis of the data.

The tracklet of an object is defined by linked detections across the short image series with  $\{\tilde{z}^{(1)}, \dots, \tilde{z}^{(k)}\}$ , where the short images series spans  $k$  epochs. Each tracklet determined as a result of the cardinality of the found objects across the images in the series is confirmed with a least-squares fit. Once each object's tracklet is confirmed, a representative measurement called a normal point  $\underline{z}$  is formed at the epoch of the last image in the series. Note that the normal point can be generated at any image epoch in the series, especially in the case where objects may be entering or exiting the scene captured by the images. The normal point  $\underline{z}$  also stores the individual detections that make up the tracklet  $\{\tilde{z}^{(1)}, \dots, \tilde{z}^{(k)}\}$  for each epoch  $k$  in the image series,

$$\underline{z}^{(k=s)} := \left\{ \begin{array}{l} z^{(s)} \\ \{\tilde{z}^{(1)}, \dots, \tilde{z}^{(k)}\} \end{array} \right\}$$
 (17)

Where the state  $z^{(s)}$  is the result of the least squares process for the chosen  $s$  epoch in the image series. The set

of normal points is defined as  $\mathcal{Z}^{(k)} = \{z_1, \dots, z_m\}$  for a cardinality of  $|\mathcal{Z}| = m$  objects in the image series.

#### 4.4.2. Orbital PHD Filter and Sensor Tasking Evaluation

The second step of the Multi-Layer PHD filter utilizes the results of the first step for all sets of image series. The classical form of the PHD filter is used with the corrector from Equation (16). For evaluation of sensor tasking the prior object catalog is used to instantiate the multi-target intensity  $D_{0|0}(\mathbf{x})$ . The aim is to determine the tracklet-to-object association only for the prior catalog, which does not require the birth process in the prediction. Therefore, only the second term of Equation (15) is used for this paper.

To perform the tracklet-to-object association, the orbital PHD filter is applied with a labeled Gaussian mixture [32, 33, 36]. The Gaussian mixture is initialized with each component of the mixture representing an object in the prior object catalog. The unique label identifier for each component is provided by the set  $\mathcal{L}_{0|0} = \{\ell_{0|0}^1, \dots, \ell_{0|0}^{n_{0|0}}\}$  for  $n_{0|0}$  initial components. Additionally, an association map for each component is generated. Where the association map stores the tracklet that is associated with a component. At the end of the GM-PHD recursion, the resulting Gaussian mixture is analyzed, where each component whose weight is greater than zero and has a non-empty association map is counted. The information from the weight is related to the likelihood of the track [36], while the association map determines tracklet association. In the case where there are two or more components with the same labels and different association maps, the component with the maximum weight is used.

## 5. SENSOR TASKING ANALYSIS AND EVALUATION

### 5.1. Observation Campaign Setup

To evaluate the observation schedules, an observation campaign was set up [24]. The campaign was performed using Purdue Optical Ground Station (POGS) located at New Mexico Skies Observatory. An observation schedule was generated for a single sensor strategy using the sensor tasking equation shown in Equation (1). The algorithm used a constant repositioning time model which assumes a constant slewing time between viewing directions. Details on a variable repositioning time model can be found in [2]. The observation schedules contain details such as the viewing directions, observation times, tracking rates, and objects predicted to be in that viewing direction.

To enable realistic observations, a minimum moon separation angle of  $20^\circ$  was set, as well as a minimum of  $5^\circ$

Sensor	RA deviation ( $^{\circ}$ )	DEC deviation ( $^{\circ}$ )	Exposure time (s)	Series length (s)	Time between series (s)
			$E$ (s)	$E$ (s)	$E$ (s)
POGS	$0.2386 \pm 0.0732$	$0.0537 \pm 0.0359$	$7.2727 \pm 0.1033$	$48 \pm 1$	$170 \pm 0.1$
			$E = 7.27$	$E = 47$	$E = 169.9880$

Table 1. Pointing and timing accuracy results based on observation campaign performed on July 13, 2024 using POGS

from the galactic plane to avoid the large density of stars near the galactic plane [24]. POGS also has a  $12^{\circ}$  minimum elevation restriction and a limiting magnitude of 16. The schedule was created for observation windows on the nights of July 13, 2024, and July 24, 2024, to observe GEO objects from the most recent TLE catalog prior to the observation window. The observations collected on the night of July 13, 2024, are the main focus of this paper. The sensor captured single exposure images with an exposure time of 7.27 seconds, in a so-called observation series. Each observation series represents a single viewing direction with five images. There were a total of 370 images taken by POGS throughout the observation window on the night of July 13, 2024, which was interrupted due to bad weather.

### 5.1.1. Timing and Pointing Accuracy

The sensor performance on the observation night was evaluated based on timing and pointing accuracies. The timing accuracy is evaluated by finding the difference between the time at which the sensor was optimally tasked and the actual time when observations took place. The mid-point of the observation series is used to perform the evaluation. The timing evaluation process helps account for any timing error the sensor may have and increases the chances that the objects predicted to be in the viewing direction are captured within the same observation series. Table 1 presents the sensor performance across different metrics compared to expected values,  $E$ , of POGS. The expected values are based on the sensor-specific calibration performed to obtain ideal sensor parameters. The sensor performance is evaluated in terms of the deviation in the optimal viewing direction, the difference in exposure times, the difference in the duration of the observation series, and the time between observation series. The actual exposure time closely matches the expected value with a small standard deviation of  $\approx 0.1s$ . Similarly, the series length and time between series are also aligned with their expected values, showing good overall consistency. These results show that POGS is highly accurate and able to target the desired viewing direction with little deviation in direction and negligible timing errors.

## 5.2. Comparison of Successfully Processed Images

The two different image processing techniques are compared and carefully analyzed. Figure 1 illustrates the number of images successfully processed by each image processing method throughout the same observation night. Each method was given the same total number of images to process. The conservative method was able to successfully process a total of 298 images, while the non-conservative method was able to successfully process 355 images.

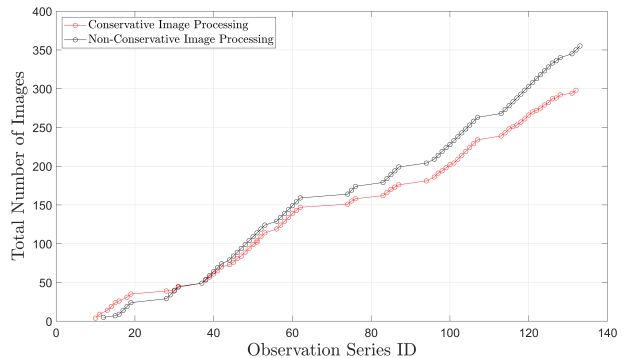


Figure 1. The cumulative number of images processed compared for each image processing method for observations by POGS on the night of July 13, 2024

Since each observation series is supposed to contain five images, it is crucial to consider how many full five-image series were captured by each processing method. The number of full five-image series is shown in Table 2. The non-conservative method results in a significantly larger number of series with five images as compared to the conservative method.

Processing Type	% of Image Series with 5 images
Conservative method	42.5
Non-conservative method	93.2

Table 2. Percentage of successful number of image series that contained the full five images as a result of the processing type

### 5.3. Conservative Image Processing Association Details

This section evaluates the sensor tasking based on the conservative image processing method and the two different association strategies. First, results from the MDA process is shown followed by the Multi-Layer PHD filter association results.

#### 5.3.1. MDA Results

The MDA method is applied on the processed images by the conservative processing approach to associate each detection in each image. Table 3 demonstrates a summary of the POGS observation results, where the MDA from Equation (14) is used to correlate detections with the TLE catalog. The results are categorized into different groups: planned objects and planned and observed objects.

Planned objects refer to objects included in the created observation schedule, while observed objects are those successfully detected by POGS and associated by the MDA. There are no new or uncataloged objects that were associated by the MDA since it relies on the TLE catalog to find the closest match to a detection.

POGS Sensor Date (UTC)	Planned objects	Planned and MDA associated objects
2024-07-13	116	114
2024-07-24	127	122

Table 3. Detection association results of MDA from conservative image processing for observation campaign performed on July 13, 2024 and July 24, 2024 using POGS

The majority of the objects planned for observation during the night were successfully associated by the MDA. On the first night on July 13, 2024, more than 98% of the planned objects in the observation schedule were matched to detections. On July 24, 2024, over 96% of the planned objects were associated. This result indicates a strong correlation between the sensor tasking observation schedule and the actual detections associated by the MDA. For the observations performed on July 13, 2024, two planned objects were not considered associated because the objects were not present in the images, or because no TLE object met the association threshold [24].

#### 5.3.2. Multi-Layer PHD Filter Results

The reduction of the number of images as a result of the conservative image processing affected the result of the image plane GM-PHD filter, where in some image series not enough information was available to produce well-defined tracklets. The image plane GM-PHD filter provided a determined presence of objects on 61.5% of the image series set from the conservative method.

Figure 3 describes the mean number of detections over the night and a comparison of the resulting cardinality from the MDA method and the GM-PHD filter. Figure 3(a) depicts the mean number of detections for each image series over the night, where only the image series that contained detections are shown. Figure 3(b) describes the comparison in cardinality, where the MDA method in all image series except one reported a higher number of objects to the GM-PHD filter. The cardinality estimate provided by the GM-PHD filter is realized from the combined information over an image series, which is shown to converge on a smaller subset of objects. In some cases, the GM-PHD filter did not converge on objects that remain persistent in at least three or more images.

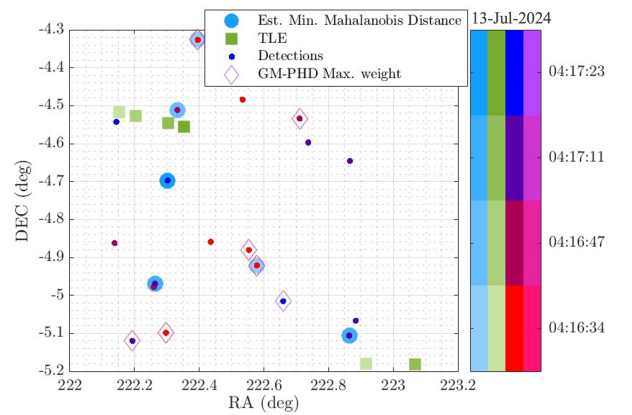


Figure 2. Result of the conservative image processing, where each set of detections from individual images is shown by the colored points according to the epoch. The predicted TLE objects are shown with the green squares, the blue filled circles represent the MDA associated detection. The maximum weighted components from the orthogonal image plane GM-PHD filter from each epoch is shown by the diamond marker.

An example of an image series where the GM-PHD filter did not determine the presence of an object is seen in Figure 2. The image series contains four images spanning from 04:17:23 to 04:16:34 UTC. The predicted TLE objects are represented by the green squares depicting the propagated catalog object location on the image plane. The GM-PHD filter resulted in a set of low-weighted components with a single association per image denoted by the diamond markers, which did not develop into a tracklet. The MDA provided a set of associated detections from each image to the TLE objects. However, the MDA of associated detections for the set of images were inconsistent with the TLE objects predicted angle rates.

The second step of the Multi-Layer PHD filter is used to determine tracklet-to-object associations. The set of the tracklets converged by the image plane GM-PHD fil-

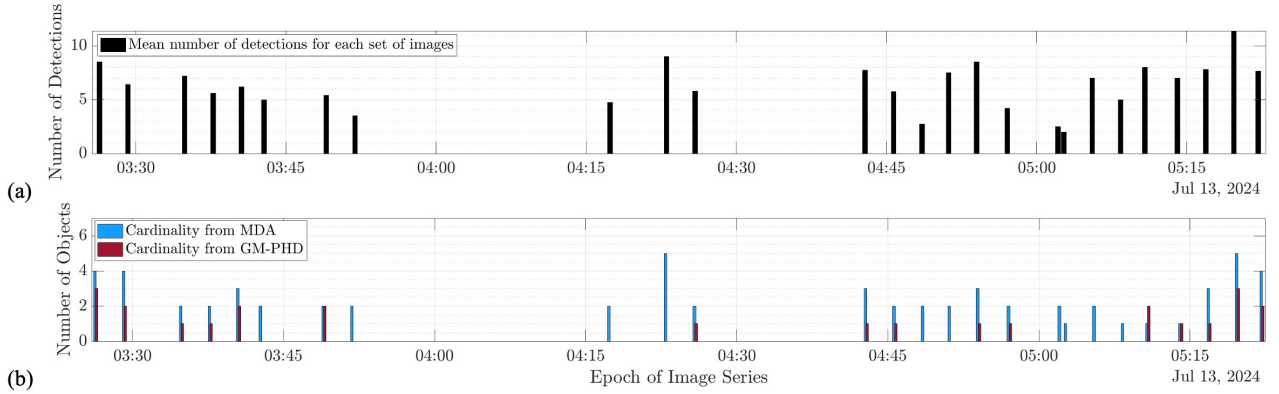


Figure 3. Results from the conservative image processing. (a) Depicts the mean number of detections as a function of time for each set of image series for observations collected on July 13, 2024. (b) Provides the captured cardinality from the MDA in blue and the cardinality determined by the image plane GM-PHD filter in red.

ter over the night of July 13, 2024 are utilized for the orbital GM-PHD filter to determine associations. The prior multi-target density is instantiated using the set of planned TLE objects with their unique identifier for the epoch at the beginning of the night. A uniform initial covariance composed of  $\sigma_x = \sigma_y = \sigma_z = 5$  km and  $\sigma_{\dot{x}} = \sigma_{\dot{y}} = \sigma_{\dot{z}} = 0.001$  km/s, is used for each object. The dynamics model for this example is expanded to include third-body perturbations for the Moon, Jupiter, and Sun, a spherical model for solar radiation pressure [9, 43] and a fourth-order spherical harmonics model [37]. The positions of the Earth, Moon Jupiter, and Sun are obtained using the Matlab Implementation of SPICE (MICE) [3] with the DE430 kernel [15]. The measurement uncertainty utilized is defined by the resulting multi-target density from the image plane GM-PHD recursion and the least-squares fit process. A resulting multi-target density from the orbital GM-PHD is decomposed to determine the associations from non-empty association maps and highest weighted components. Table 4 describes the comparison in cardinality defined by the single image detection with MDA and the cardinality of object association from well-defined tracklets with Multi-Layer PHD filter. It is seen that only 17% of the planned objects were associated with the generated tracklets. The where tracklet-to-object association requires a minimum of three detections for each tracklet before an association with an object is made. In the case of the conservative image processing, the number of successfully processed image series with five images as seen in Table 2 contributed to the relatively low cardinality.

POGS Sensor Date (UTC)	Object Association Cardinality	
07-13-2024	MDA	114
	Multi-Layer PHD	20

Table 4. Cardinality results of MDA and the Multi-Layer PHD filter from conservative image processing for observation campaign performed on July 13, 2024 using POGS.

#### 5.4. Non-Conservative Image Processing Association Details

Similar to the conservative processing evaluation, this section analyzes the sensor tasking based on the non-conservative image processing using the two association strategies.

##### 5.4.1. MDA Results

Despite the increase in the number of detections in all images, which gives more measurements to correlate, the MDA did not associate any additional TLE objects compared to the result from the conservative method shown in Table 3. This outcome shows that the MDA implemented is not influenced by the number of images or detections in each observation series. The same two objects that were planned for observation remain unassociated by the MDA using both image processing methods.

##### 5.4.2. Multi-Layer PHD Results

In the non-conservative approach, a larger number of images were processed, resulting in a higher number of detections per image. Figure 4 describes the mean number of detections and the comparison of the cardinality of objects determined by the MDA and the image plane GM-PHD filter for the non-conservative image processing. In Figure 4(a) the mean number of detections for the set of image series often surpasses 100 detections, where in contrast to Figure 3(a) the mean number of detections only reaches a maximum of 10. It was seen that the number of image series achieved a greater epoch range for the night, and all image series contained enough images for the image plane GM-PHD to analyze.

However, it is seen that later in the night, after

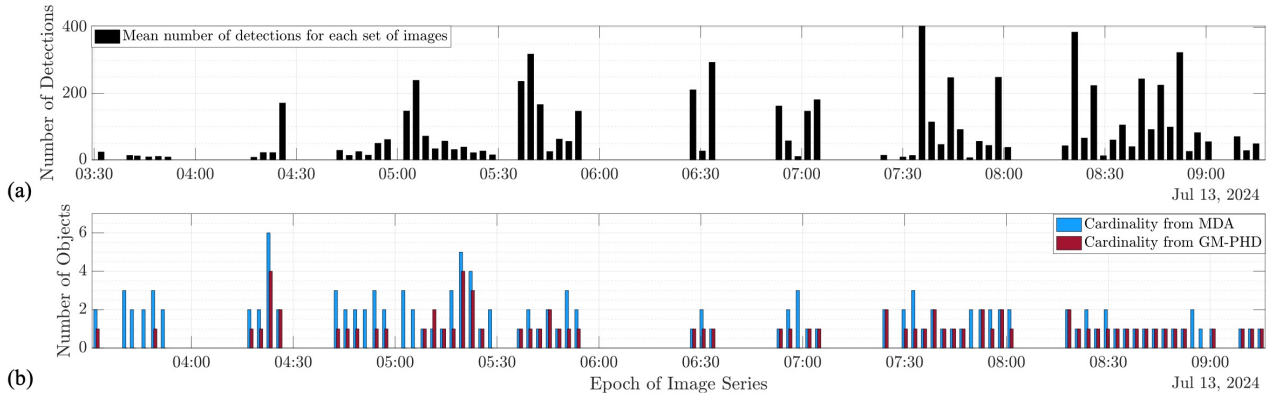


Figure 4. Results from the non-conservative image processing. (a) Depicts the mean number of detections as a function of time for each set of image series for observations collected on July 13, 2024. (b) Provides the captured cardinality from the MDA method in blue and the cardinality determined by the image plane GM-PHD filter in red.

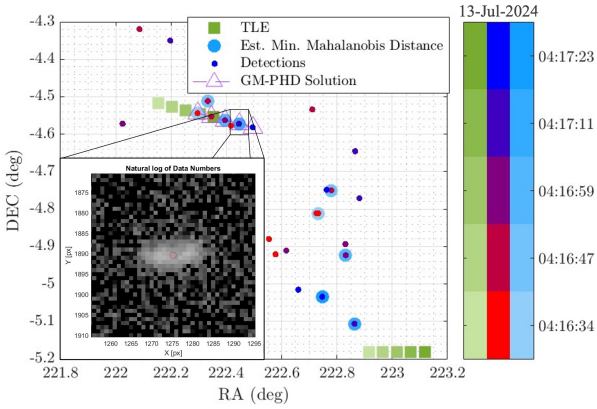


Figure 5. Result of the non-conservative image processing, where each set of detections from individual images is shown by the colored points according to the epoch. The predicted TLE objects are shown with the green squares, the blue filled circles represent the MDA associated detection. The tracklet solution from the orthogonal image plane GM-PHD filter is denoted by the linked magenta triangles.

07:30 UTC there was a reduction in the difference in the estimated cardinality between MDA and the image plane GM-PHD. In Figure 4(b), for the 73 image series the image plane GM-PHD the convergence rate on objects is increased to 83.6% compared to the 61.5% from the conservative approach. The cardinality estimated by the image plane GM-PHD filter remains in most cases below the estimated cardinality determined by the MDA. Figure 5 shows the solution of the image plane GM-PHD filter for the same image series shown in Figure 2, where in the case of the non-conservative method, the five images are available. The additional set of detections revealed a coherent set of detections near the predicted TLE object on the upper left of the plot.

The tracklet solution of the image plane GM-PHD filter is denoted by the linked magenta triangles, where the MDA associated the same three of five detections for the tracklet. To further verify the validity of the measurements obtained from the GM-PHD filter, spot-checking was conducted on each converged detection. An example of this verification process is shown in Figure 5, where a specific detection is marked as a red circle and zoomed in from the raw image.

Figure 6 illustrates an image series in which the image plane GM-PHD converged on two objects. The tracklet for each object is shown to be consistent with the predicted motion of the TLE objects in the image plane over the set of images.

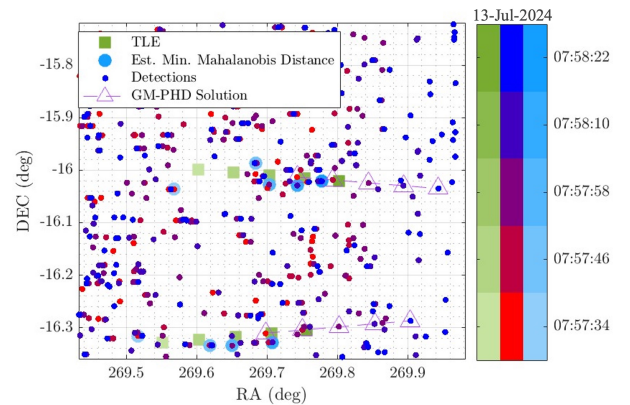


Figure 6. Example of non-conservative image processing, where the image plane GM-PHD filter converges on two objects, denoted by the linked triangle markers. Detections are shown with epoch colored points, predicted TLE objects are shown by the green squares and MDA detections are shown by blue filled circles.

The MDA did not associate with the same detections for each image determined by the image plane GM-PHD filter. Despite the large number of detections, the image plane GM-PHD filter displayed robust behavior in converging on objects present in all five images.

From the outcome of each image processing method, a set of epoch-matching images of the converged image plane PHD filter were selected for comparison. Figure 7 describes the comparison of the two methods for the number of detections and also the results of the orthogonal image plane GM-PHD filter.

Figure 7(a) provides the number of detections for images of the same epoch. It was seen that with the non-conservative method, the first 19 epoch-matching images have an increase of two to three times more detections.

For the remaining 61 epoch-matching images, the number of detections for the non-conservative method is increased in most to at least an order of magnitude or more. Figure 7(b) compares the solution of the orthogonal image plane GM-PHD for the image series to which each image number belongs. For the first set of 10 images, the solution of the filter provided a reduced object cardinality in the non-conservative image processing method. It was noted that the increase in the number of detections did not always guarantee a filter solution. An example of this is shown with epoch-matching image numbers 49 to 54, where neither image processing method resulted in an object despite a large number of detections present.

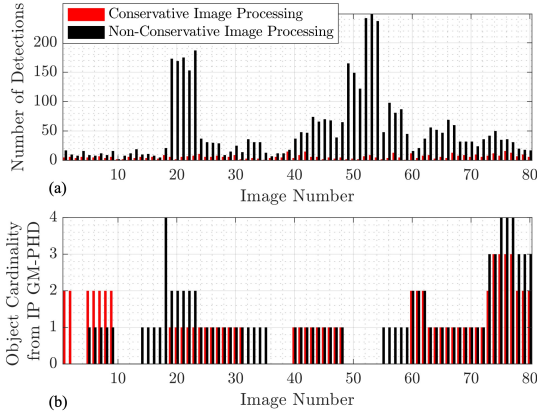


Figure 7. (a) For images of the same epoch, the number of detections for the conservative mode is shown in red and non-conservative mode depicted in black. (b) The cardinality solution from the image plane (IP) GM-PHD for the conservative and non-conservative mode are also shown in the same color order.

The second step of the Multi-Layer PHD was performed with the resulting tracklets defined by the image plane GM-PHD filter with the same initialized labeled Gaussian mixture and dynamics modeling as described in Section 5.3.2. Table 5 provides a comparison in cardinality

using the non-conservative image processing between the MDA object-to-detection association and the Multi-Layer PHD filter object-to-tracklet association. The increase in object association provided by the Multi-layer PHD is increased primarily due to the higher number of successfully processed image series from the non-conservative image processing.

POGS Sensor Date (UTC)	Object Association Cardinality	
07-13-2024	MDA	114
	Multi-Layer PHD	61

Table 5. Cardinality results of MDA and the Multi-Layer PHD filter from non-conservative image processing for observation campaign performed on July 13, 2024 using POGS.

For the 61 objects that were associated by the Multi-Layer PHD filter with the tracklets produced from the non-conservative image processing, 60 objects were identified as optimally tasked from the TLE object catalog. The 60 objects result in 51% of optimally tasked objects were observed. A single object was not optimally tasked but was included in the TLE catalog. The same object was also associated with the MDA method.

## 5.5. Sensor Tasking Evaluation Summary

The cardinality results from the conservative and non-conservative image processing techniques, shown in Tables 4 and 5 respectively, demonstrate the effectiveness of each association strategy in associating detections. A summary of the cardinality for the Multi-Layer PHD filter and MDA is shown in Table 6 for both conservative and non-conservative image processing methods. The MDA successfully associates a larger number of the optimally planned objects as compared to the Multi-Layer PHD filter. However, the Multi-Layer PHD filter resulting cardinality is a tracklet-to-object association, where the MDA cardinality represents the detection-to-object association.

POGS Sensor Date (UTC)		Object Association Cardinality	
		MDA	Multi-Layer PHD
07-13-2024	Conservative	114	20
	Non-Conservative	114	61

Table 6. Comparison of the cardinality results from the MDA and the Multi-Layer PHD on both the conservative and non-conservative image processing methods for the observation campaign on July 13, 2024.

The differences between the two association strategies are provided in a set of pictographic illustrations shown in Figure 8. The process of the orthogonal image plane

GM-PHD filter is denoted in (a) and the MDA is denoted in (b). In Figure 8(a) a tracklet acquisition across the set of images in the same observation series is represented by the linked purple triangles. In Figure 8(b), the MDA is performed on each detection in each independent image to associate the detection shown in blue to the predicted TLE object on the image plane in green.

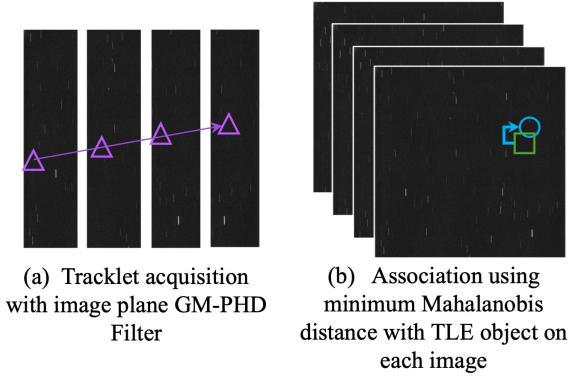


Figure 8. (a) Denotes the process of taking each closely space image in time and using the orthogonal image plane GM-PHD filter to determine tracklets. (b) Shows the process of the MDA for association of a detection in blue to the TLE object in green for each image independently.

For the image series in which the Multi-Layer PHD filter determined the presence of objects in the set of image series, the number of detections per associated object was analyzed. The comparison shown in Table 7 illustrates the maximum and minimum number of detections per associated object between the MDA and Multi-Layer PHD filter seen for the observation campaign on July 13, 2024. For all tracklet solutions found with the image plane GM-PHD the smallest and largest tracklet by number of detections was found to be the same for both the conservative and non-conservative image processing methods. The association to an object resulting from the orbital labeled GM-PHD filter attributes a group of detections defined by the tracklet to a prior catalog object estimate. Therefore, the cardinality shown in Table 6 for the Multi-Layer PHD filter represents the observed objects over multiple images in an image series. Unlike the Multi-Layer PHD filter, the MDA process does not form a tracklet of detections. Instead, it utilizes a single detection basis for each image in an observation series, resulting in only one object association per detection. The MDA object association cardinality of 114 out of the 116 planned objects presented in Table 6 is purely reliant on the TLE catalog and the associations are performed in a single image. Inaccuracies in the TLE data can lead to discrepancies in the propagation and association process [22]. These errors highlight the need to account for velocity probabilities during the association process to provide results using an approach that does not depend on TLE sets.

POGS Sensor Date (UTC)	Number of Detections per Object Associated (min, max)		
		MDA	Multi-Layer PHD
07-13-2024	Conservative	1	3, 5
	Non-Conservative	1	3, 5

Table 7. Comparison between the number of detections per object associated determined by the MDA and the Multi-layer PHD filter for both conservative and non-conservative image processing methods over the observation campaign on July 13, 2024.

The solutions provided by the Multi-Layer PHD filter are confirmed with a spot-checking process conducted on the detections in the tracklets determined by the image-plane GM-PHD filter. An example of this is shown in Figure 5 and Figure 9 where the blue star marker represents the same zoomed-in detection in Figure 5. This process demonstrates that the identified detection is not a star streak but is more likely to be an object, confirming that it is a valid candidate for association. It also provides additional confidence in the accuracy of the GM-PHD filter in distinguishing object detections from background noise and stellar sources.

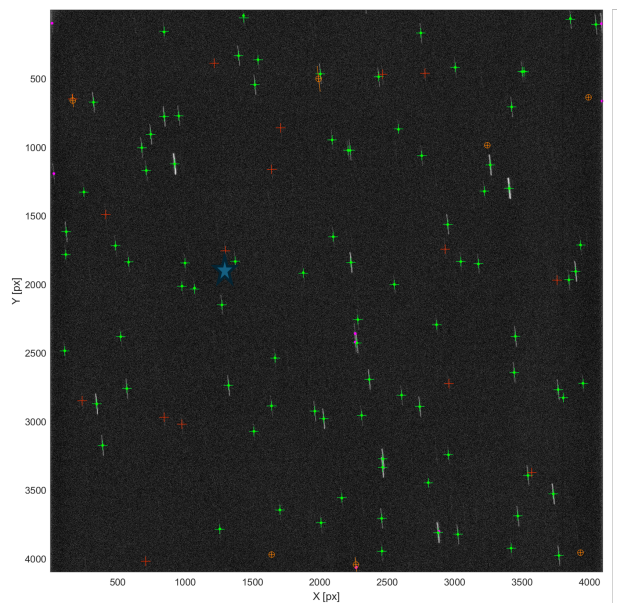


Figure 9. Raw FITS Image. The green markers represent matched star streak detections and orange circles are the possible object detections. Unmatched streaks or measurements are shown as red +.

## 6. CONCLUSIONS

In this paper, a sensor tasking framework and validation methods were explored, which used two different image

processing methods and two different association methods.

A greedy optimizer was implemented to solve the sensor tasking problem, resulting in computationally efficient observation schedules for optical observations using a single ground-based optical sensor, observing the geosynchronous regions. The observation schedule is a fixed, open-loop setup. Tasking plans were created adhering to a set of visibility conditions that allow a more realistic application of the sensor tasking algorithm to real-life ground-based observers. Two observation campaigns were conducted on July 13, 2024, and July 24, 2024. The images captured by Purdue Optical Ground Station (POGS) were processed using two methods. The conservative method resulted in fewer detections compared to the non-conservative method.

Two methods of validating the success of the sensor tasking were used for the observation campaign of July 13, 2024. The detections from each image processing method were used to perform associations. The first validation method was accomplished with the Mahalanobis Detection Association (MDA) technique, which was utilized to associate the detections on each image to a space object catalog. The MDA method remained unaffected by the image processing method, providing the same majority of associated objects present in the viewing directions. The second method of validation of the sensor tasking was done with the Multi-Layer Probability Hypothesis Density (PHD) filter. The Multi-Layer PHD filter generated tracklets before performing association to an object. The detections across images are associated, which generated tracklets by the orthogonal image plane Gaussian mixture PHD (GM-PHD). The image plane GM-PHD filter generated a different number of converged objects with well-defined tracklets for the two image processing methods. The increased number of images in the non-conservative image processing revealed an increase in the number of converged objects compared to the conservative image processing. The set of additional detections allowed the orthogonal image plane GM-PHD filter to determine the presence of objects with appropriate angle rates according to the predicted motion of the TLE objects in the image plane. The tracklet-to-object association was performed by the labeled orbital GM-PHD filter with the generated tracklets. The planned TLE objects were used to initialize the prior multi-target density. The labeled orbital GM-PHD indicated that all objects except one were identified as part of the optimal tasking.

The effectiveness of the sensor tasking was demonstrated by the execution of the observation campaign and the two association methods, which produced different successful results. POGS, the sensor used in the observation campaign, showed a small standard deviation in exposure time of 0.1 seconds, and negligible errors in series length and time between series. POGS also displayed high accuracy in targeting the desired viewing directions. The validation of the sensor tasking with the MDA, a detection-to-object association, indicated over 96% success of observed to planned objects. The tracklet-to-

object association made with the Multi-Layer PHD filter resulted in a success of 17% of observed to planned objects for conservative image processing and 51% for non-conservative image processing. The tracklet-to-object association, which accounts for the association of the group of detections in an image series, provided a stronger result. In contrast, the detection-to-object association only requires a single detection, which is heavily reliant on an object catalog and can be affected by catalog data.

## REFERENCES

- (2018). Reprint of: Mahalanobis, P.C. (1936) "On the Generalised Distance in Statistics." *Sankhya A*, 80(S1):1–7.
- Abdulrahman Abdrabou (2025). Unraveling the moving sky: Optimizing Sensor Tasking for Space Situational Awareness.
- Acton, C. (1998). An overview of SPICE. *Jet Propulsion Laboratory: Oak Grove, KY, USA*.
- Africano, J., Schildknecht, T., Matney, M., Kervin, P., Stansbery, E., and Flury, W. (2000). A Geosynchronous Orbit Search Strategy. *Space Debris*, 2(4):357–369.
- Anz-Meador, P., Opiela, J., and Liou, J.-C. (2023). History of on-orbit satellite fragmentations. Technical report.
- Baietto, N. J. (2022). Space Object Correlation Between the Space-Track and Vimpel Catalogs. page 5403592 Bytes. Artwork Size: 5403592 Bytes Publisher: Purdue University Graduate School.
- Bar-Shalom, Y. (1978). Tracking methods in a multitarget environment. *IEEE Transactions on Automatic Control*, 23(4):618–626.
- Bar-Shalom, Y. (1990). *Multitarget-multisensor tracking: advanced applications*. Artech House, Boston.
- Beutler, G. (2004). *Methods of celestial mechanics: Volume II: Application to planetary system, geodynamics and satellite geodesy*. Springer Science & Business Media, Berlin, Heidelberg.
- Binney, J. and Tremaine, S. (2008). *Galactic dynamics*. Princeton series in astrophysics. Princeton University Press, Princeton, 2nd ed edition.
- Blackman, S. (2004). Multiple hypothesis tracking for multiple target tracking. *IEEE Aerospace and Electronic Systems Magazine*, 19(1):5–18.
- Blackman, S. S. and Popoli, R. (1999). *Design and analysis of modern tracking systems*. Artech House radar library. Artech House, Boston. Publication Title: Design and analysis of modern tracking systems.
- Carolyn Frueh, Thomas Schildknecht, Reto Musci, and Martin Ploner (2009). CATALOGUE CORRELATION OF SPACE DEBRIS OBJECTS.
- ESA (2023). ESA'S Annual Space Environment Report. Technical report, ESA Space Debris Office.

15. Folkner, W. M., Williams, J. G., Boggs, D. H., Park, R. S., and Kuchynka, P. (2014). The planetary and lunar ephemerides DE430 and DE431. *Interplanetary network progress report*, 196(1):42–196.
16. Fortmann, T., Bar-Shalom, Y., and Scheffe, M. (1983). Sonar tracking of multiple targets using joint probabilistic data association. *IEEE Journal of Oceanic Engineering*, 8(3):173–184.
17. Frueh, C., Fiedler, H., and Herzog, J. (2016). Realistic Sensor Tasking Strategies.
18. Frueh, C., Fiedler, H., Schildknecht, T., and Herzog, J. (2021). Multi-Target Tracking for SMARTnet: Multi-Layer Probability Hypothesis Filter for Near-Earth Object Tracking. In *8th European Conference on Space Debris*.
19. Frueh, C., Fiedler, H., and Herzog, J. (2018). Heuristic and Optimized Sensor Tasking Observation Strategies with Exemplification for Geosynchronous Objects. *Journal of Guidance, Control, and Dynamics*, 41(5):1036–1048.
20. Frueh, C., Paul, S. N., and Fiedler, H. (2017). Sensor Tasking for Detection and Custody of HAMR Objects.
21. Frueh, Carolin (2022). AAE 590 Space Traffic Management. *School of Aeronautics and Astronautics, Purdue University*.
22. Früh, C. and Schildknecht, T. (2012). Accuracy of Two-Line-Element Data for Geostationary and High-Eccentricity Orbits. *Journal of guidance, control, and dynamics*, 35(5):1483–1491. Place: Reston, VA Publisher: American Institute of Aeronautics and Astronautics.
23. Gutierrez, J. and Frueh, C. (2025). A Data-Driven Probability Hypothesis Filter for Space Situational Awareness.
24. Herzog, J., Abdrabou, A., Fiedler, H., and Frueh, C. (2024). Test Campaign of the Optimized Maintenance and Survey Tasking (OMST) Strategy with Multiple Telescope Stations. In *22nd IAA Symposium on Space Debris*, pages 1769–1779, Milan, Italy. International Astronautical Federation (IAF).
25. Hill, K., Alfriend, K., and Sabol, C. (2008). Covariance-Based Uncorrelated Track Association. In *AIAA/AAS Astrodynamics Specialist Conference and Exhibit*, Honolulu, Hawaii. American Institute of Aeronautics and Astronautics.
26. Holzinger, M. J., Scheeres, D. J., and Alfriend, K. T. (2012). Object Correlation, Maneuver Detection, and Characterization Using Control Distance Metrics. *Journal of Guidance, Control, and Dynamics*, 35(4):1312–1325.
27. Houtz, N. and Frueh, C. (2018). STREAK DETECTION AND CHARACTERIZATION IN GROUND-BASED OPTICAL OBSERVATIONS OF SPACE OBJECTS.
28. Houtz, N. K. (2024). *Image Processing Pipeline and a Global Search for Local Maxima Method of Object Detection*. PhD Thesis, Purdue University.
29. Little, B. D. (2019). Optical Sensor Tasking Optimization for Space Situational Awareness. page 26237866 Bytes. Artwork Size: 26237866 Bytes Publisher: Purdue University Graduate School.
30. Little, B. D. and Frueh, C. (2018). SSA Sensor Tasking: Comparison of Machine Learning with Classical Optimization Methods. *Purdue University School of Aeronautics and Astronautics*, page 17.
31. Little, B. D. and Frueh, C. E. (2020). Space Situational Awareness Sensor Tasking: Comparison of Machine Learning with Classical Optimization Methods. *Journal of Guidance, Control, and Dynamics*, 43(2):262–273.
32. Mahler, R. P. S. (2007). *Statistical multisource-multitarget information fusion*. Artech House information warfare library. Artech House, Boston, 1st ed. edition. Publication Title: Statistical multisource-multitarget information fusion.
33. Mahler, R. P. S. (2014). *Advances in statistical multisource-multitarget information fusion*. Artech House electronic warfare library. Artech House, Boston, 1st ed. edition. Publication Title: Advances in statistical multisource-multitarget information fusion.
34. Musci, R., Schildknecht, T., and Ploner, M. (2004). Orbit improvement for GEO objects using follow-up observations. *Advances in Space Research*, 34(5):912–916.
35. NASA (2015). NASA Technology Roadmaps - Introduction, Crosscutting Technologies, and Index. *NASA*.
36. Panta, K., Clark, D. E., and Vo, B.-N. (2009). Data Association and Track Management for the Gaussian Mixture Probability Hypothesis Density Filter. *IEEE Transactions on Aerospace and Electronic Systems*, 45(3):1003–1016.
37. Pines, S. (1973). Uniform representation of the gravitational potential and its derivatives. *AIAA Journal*, 11(11):1508–1511.
38. Reid, D. (1979). An algorithm for tracking multiple targets. *IEEE Transactions on Automatic Control*, 24(6):843–854.
39. Rose, M. J. (2020). Optical Sensor Uncertainties and Variable Repositioning Times in the Single and Multi-Sensor Tasking Problem. page 25345238 Bytes. Artwork Size: 25345238 Bytes Publisher: Purdue University Graduate School.
40. Schildknecht, T. (2007). Optical surveys for space debris. *The Astronomy and Astrophysics Review*, 14(1):41–111.
41. Schildknecht, T., Hugentobler, U., and Ploner, M. (1999). Optical surveys of space debris in GEO. *Advances in Space Research*, 23(1):45–54.
42. Space-Track (2025). Space-Track.
43. Vallado, D. A. (2022). *Fundamentals of astrodynamics and applications*. Number 21 in Space technology library. Microcosm Press, Torrance, CA, fifth edition, first printing edition.

44. Vo, B.-n., Mallick, M., Bar-Shalom, Y., Coraluppi, S., Osborne, R., Mahler, R., and Vo, B.-t. (2015). Multitarget tracking. *Wiley encyclopedia of electrical and electronics engineering*. Publisher: Wiley Hoboken, NJ, USA.